A soluble α-synuclein construct forms a dynamic tetramer

Wei Wang[a,b,1], Iva Perovic[c,1], Johnathan Chittuluru[d], Alice Kaganovich[e], Linh T. T. Nguyen[a,b], Jingling Liao[a,b], Jared R. Auclair[c], Derrick Johnson[a,b], Anuradha Landeru[a,b], Alana K. Simorellis[f], Shulin Ju[f], Mark R. Cookson[e], Francisco J. Asturias[d], Jeffrey N. Agar[c], Brian N. Webb[g], ChulHee Kang[g], Dagmar Ringe[f,h,2], Gregory A. Petsko[f,h,2], Thomas C. Pochapsky[f,2], and Quyen Q. Hoang[a,b,2]

[a]Department of Biochemistry and Molecular Biology, and [b]Stark Neurosciences Research Institute, Indiana University School of Medicine, Indianapolis, IN 46202; [f]Department of Chemistry and Biochemistry and Rosenstiel Basic Medical Sciences Research Center, and [c]Department of Chemistry and Rosenstiel Basic Medical Sciences Research Center, Brandeis University, Waltham, MA 02454; [d]Department of Cell Biology, The Scripps Research Institute, La Jolla, CA 92307; [e]Laboratory of Neurogenetics, National Institutes of Health, Bethesda, MD 20892; [g]Department of Chemistry, Washington State University, Pullman, WA 99164; and [h]Department of Neurology and Center for Neurologic Diseases, Harvard Medical School and Brigham and Women's Hospital, Cambridge, MA 02139

Contributed by Gregory A. Petsko, September 19, 2011 (sent for review April 28, 2011)

A heterologously expressed form of the human Parkinson disease-associated protein α-synuclein with a 10-residue N-terminal extension is shown to form a stable tetramer in the absence of lipid bilayers or micelles. Sequential NMR assignments, intramonomer nuclear Overhauser effects, and circular dichroism spectra are consistent with transient formation of α-helices in the first 100 N-terminal residues of the 140-residue α-synuclein sequence. Total phosphorus analysis indicates that phospholipids are not associated with the tetramer as isolated, and chemical cross-linking experiments confirm that the tetramer is the highest-order oligomer present at NMR sample concentrations. Image reconstruction from electron micrographs indicates that a symmetric oligomer is present, with three- or fourfold symmetry. Thermal unfolding experiments indicate that a hydrophobic core is present in the tetramer. A dynamic model for the tetramer structure is proposed, based on expected close association of the amphipathic central helices observed in the previously described micelle-associated "hairpin" structure of α-synuclein.

dynamic structure | helical | Parkinson's disease | NMR | heteronuclear single-quantum coherence

The protein α-synuclein (αSyn) is associated with the two most prevalent neurodegenerative diseases, Parkinson disease (PD) and Alzheimer's disease (AD). The presence of αSyn-rich aggregates (Lewy bodies) in neurons of the *substantia nigra* is the defining histopathological hallmark of PD, and is used to differentiate PD from other neurological disorders (1). Monogenic point mutations (A30P, A53T, and E46K) as well as gene duplication and triplication of the αSyn locus have been identified as causal factors of early onset familial PD; E46K has also been associated with Lewy body dementia, the second most common form of dementia after AD (2–4).

αSyn is small (140 residues), and though the C-terminal region (~residues 100–140) is highly acidic and expected to be disordered, the first 100 residues are predicted to be structured and to have α-helical propensity (*SI Appendix*, Fig. S1). Stable helical structures have been detected by circular dichroism (CD) and NMR when αSyn is incubated with detergent micelles and lipid vesicles (5, 6). Soluble αSyn is typically referred to as an "intrinsically disordered" protein (7, 8). However, we herein report the biophysical characterization of a purified soluble form of αSyn that is oligomeric and fractionally occupies helical structures in the absence of micelles or vesicles. The αSyn construct used in our work is purified by use of an N-terminal GST affinity tag under mild conditions to preserve any native structure. After removal of the GST tag, a 10-residue N-terminal extension remains on the αSyn. However, the similarity of the $^{1}H,^{15}N$ heteronuclear single-quantum coherence (HSQC) fingerprint of our αSyn construct (*SI Appendix*, Figs. S2 and S3) to those reported by other groups for αSyn suggests that the N-terminal extension does not change structural tendencies significantly. The αSyn construct described here is not toxic to membranes or cells, does not readily aggregate or form amyloid-like fibrils, and forms transient ordered structures characteristic of a dynamically folded molecule whose secondary structural features are stabilized by oligomerization. In independent studies, Bartels et al. (9) report that a tetrameric form of αSyn with properties similar to those reported here is the predominant soluble form of the protein in brain and red blood cells.

Results

The αSyn construct described here was expressed in *Escherichia coli* as a GST fusion protein. To preserve any quaternary structure of αSyn, denaturing conditions were avoided throughout purification. Unless otherwise noted, protein purification, characterization, and storage all made use of the same buffer [100 mM Hepes (pH 7.4), 150 mM NaCl, 10% glycerol, and 0.1% n-octyl-β-glucopyranoside (BOG)]. We note that 0.1% BOG (~3 mM) is an order of magnitude below the critical micelle concentration of this detergent (~25 mM). After the GST tag is removed proteolytically, the construct retains a 10-residue N-terminal fragment (GPLGSPEFPG) that is part of the protease recognition site. However, for convenience in comparing with published work, the canonical sequence numbering is used here. The construct can be purified to homogeneity on a size-exclusion column, and elutes as a single sharp peak with an apparent molecular weight (M_r) of ~56,000, ~3.6-times the expected molecular weight of the αSyn construct (M_r of 15,397; Fig. 1*A*). Chemical cross-linking of the purified construct shows four bands on SDS/PAGE gels, suggesting that a tetramer is present (Fig. 1*B*). The isolated cross-linked bands were analyzed by MALDI-TOF mass spectrometry, which confirmed that the two major bands correspond to a trimer and tetramer of αSyn

Author contributions: W.W., I.P., M.R.C., F.J.A., J.N.A., C.K., D.R., G.A.P., T.C.P., and Q.Q.H. designed research; W.W., I.P., J.C., A.K., L.T.T.N., J.L., J.R.A., D.J., A.L., A.K.S., S.J., F.J.A., B.N.W., T.C.P., and Q.Q.H. performed research; S.J., M.R.C., J.N.A., T.C.P., and Q.Q.H. contributed new reagents/analytic tools; W.W., I.P., J.C., A.K., L.T.T.N., J.L., J.R.A., D.J., A.L., A.K.S., S.J., M.R.C., F.J.A., J.N.A., B.N.W., C.K., D.R., G.A.P., T.C.P., and Q.Q.H. analyzed data; and D.R., G.A.P., T.C.P., and Q.Q.H. wrote the paper.

The authors declare no conflict of interest.

Freely available online through the PNAS open access option.

Data deposition: Chemical shift assignments for the αSyn construct have been deposited in the BioMagResBank, http://www.bmrb.wisc.edu/ (accession no. 17665).

[1]W.W. and I.P. contributed equally to this work.

[2]To whom correspondence may be addressed. E-mail: petsko@brandeis.edu, qqhoang@iupui.edu, ringe@brandeis.edu, or pochapsk@brandeis.edu.

This article contains supporting information online at www.pnas.org/lookup/suppl/doi:10.1073/pnas.1113260108/-/DCSupplemental.

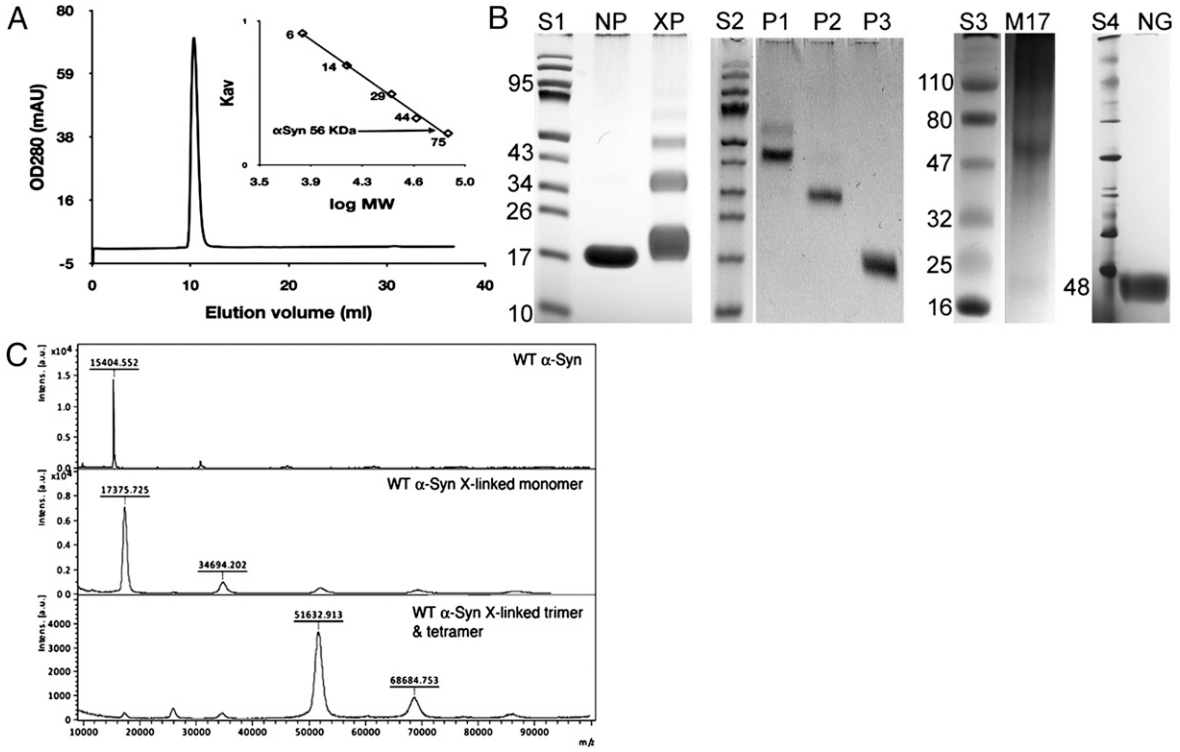

Fig. 1. Oligomeric states of αSyn. (*A*) Elution profile of purified αSyn construct from Superdex75 column. (*Inset*) Calibration curve used for size estimates. (*B*) S1 to S4 are molecular weight standards. NP, native purified αSyn; XP, αSyn cross-linked with glutaraldehyde. P1, P2, and P3 are purified cross-linked tetramer, trimer, and monomer, respectively. M17, cross-linked lysate of neuroblastoma cell line M17 overexpressing WT human αSyn. NG, Blue Native PAGE of purified recombinant αSyn (48 refers to the lowest NG band). For analysis of gels, see *SI Appendix*, Fig. S1. (*C*) MALDI-TOF spectra of αSyn (*Top*, calculated M_r = 15,397), cross-linked monomer and dimer (*Middle*, 17 kDa and 35 kDa), and cross-linked trimer and tetramer (*Bottom*, 52 kDa and 68 kDa).

(Fig. 1*C*). For comparison, we also cross-linked the cell lysate of neuroblastoma cells (M17) expressing wild-type αSyn and found a predominant band with an apparent molecular weight ∼4× that of single-chain αSyn. Nondenaturing Blue Native PAGE (Invitrogen) gels of our construct exhibit one prominent band with an apparent M_r of 48,000 (Fig. 1*B*), at an apparent molecular weight ∼3.2× the molecular weight of monomeric αSyn. Though native gels are not reliable for molecular weight estimation (10), the native gel indicates that the purified construct is largely homogeneous.

αSyn oligomers were characterized using single-particle EM. EM images of αSyn particles recorded after staining showed that the majority of particles were of similar size (Fig. 2*A*). Reference-free alignment and clustering of individual images indicated that the particles had reasonably well-defined features despite their small size, and suggested a repeating feature. However, glycerol (10% vol/vol) present in the original samples interfered with staining and complicated further image analysis. Removal of glycerol causes some increase in heterogeneity, although well-defined particles were still dominant (Fig. 2*B*). Alignment and clustering of ∼19,000 glycerol-free αSyn particle images yielded three groups of slightly different size. Gaussian-edged circular templates matching the sizes of these initial averages were used as references for competitive cross- correlation matching to separate particles by size into three groups. Reference-free alignment and *k*-means clustering were used to further classify images within each group. Averages with distinct features were obtained from all three groups (Fig. 2*C*). Small- particle averages showed three V-shaped repeating features that resemble arrowheads pointing at each other, arranged in a threefold symmetrical configuration (Fig. 2*D*). Medium-particle averages were composed of four of the same repeating units, arranged in a fourfold symmetrical configuration (Fig. 2*E*). Averages from the large particles are harder to interpret but appear to correspond to some superposition of the oligomeric arrangements. We conclude that all averages represent oligomeric forms of αSyn, with each repeating unit likely corresponding to an individual αSyn monomer. The small and medium EM averages are consistent with homotrimeric and homotetrameric species, respectively. The medium size group (tetramer) was nearly twofold more abundant than the small group (trimer). This result, taken together with all data presented above, leads us to believe

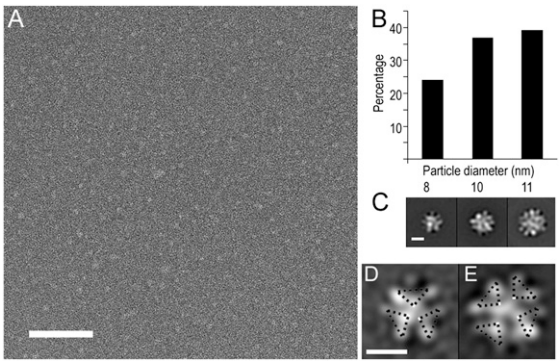

Fig. 2. Electron microscopy analysis of purified recombinant αSyn. (*A*) Image of particles preserved in stain. (Scale bar, 100 nm.) (*B*) Distribution of particle sizes after glycerol removal. (*C*) Overall class averages obtained from the small-, medium-, and large-sized particle groups. (Scale bar, 5 nm.) (*D* and *E*) Representative class averages from the small- and medium-sized particle groups. (Scale bar, 5 nm.) Symmetry units shown as dashed triangles over the EM class averages.

that the αSyn purified from the 56-kDa peak in Fig. 1*A* represents primarily a homotetramer.

CD spectra of the αSyn construct exhibit negative bands at 222 nm and 208 nm, and a positive band at 193 nm (Fig. 3*A*), characteristic of a protein containing 65% α-helix, 17% turns, and 8% unfolded, as calculated with DichroWeb (11) using two different algorithms, SELCON3 (12) and CONTIN (13). A ThermoFluor assay (14) was used to monitor thermal unfolding of αSyn, and to detect whether a hydrophobic core is present in the oligomer, as determined by an increase in fluorescence emitted by the dye present. We observed a sigmoidal unfolding curve for the αSyn construct, indicating a cooperative unfolding with exposure of hydrophobic residues (*SI Appendix*, Fig. S4). Taken together, the CD and fluorescence data indicate that αSyn oligomer consists of subunits held together by hydrophobic interactions.

We used solution NMR to localize the transient formation of α-helices in αSyn. Resonance assignments were made using standard methods [HNCO, HN(CO)CA, HNCA, HNCACB, ^{15}N-edited NOESY, and TOCSY]. A comparison of our assignments with those made for αSyn upon association with lipid (which drives helix formation) shows somewhat decreased chemical shift dispersion in the present case, indicating that helix formation is dynamic (15, 16). Rather, our ^{1}H,15N HSQC spectra (*SI Appendix*, Figs. S2 and S3) resemble those of wild-type αSyn in living *E. coli* cells obtained using in vivo NMR methods by McNulty et al. (17). Chemical shift-based secondary structural analysis using TALOS+ (18) indicates that with the exception of short segments near the N terminus of the polypeptide, the structure of the peptide is dynamic (*SI Appendix*, Fig. S5). Although a high degree of spectral overlap is present even in 3D data sets, we were able to identify a sufficient number of sequential (Hα-HN *i*, *i* +3) NOEs in ^{15}N-edited NOESY spectra to confirm the transient existence of α-helical structure between residues Phe4-Thr43 (α1) and His50-Asn103 (α2; *SI Appendix*, Fig. S6). In many cases, these NOEs are quite weak, consistent with fractional occupancy. Analysis of Cα and Hα shifts in terms of fractional secondary structure population indicate that the α1 region contains shorter discrete sections with helical tendency: residues 4 to 16 yield a 22% helical tendency based on predicted Cα shifts (6.5% from Hα), a 28% tendency for residues 20 to 23 (17% from Hα), and random coil (−10% helical tendency from Cα shifts, −0.2% from Hα) for residues 32 to 43 (*SI Appendix*, Fig. S7) (19–21). The same chemical shift analysis predicts more uniform helix occupancy in the α2 region (13% based on Cα and 20% from Hα for residues 48–90). For the C-terminal of αSyn (residues 104–140), both chemical shift averages predict random structure (<1% helix). In recent studies of short αSyn N-terminal peptides fused to maltose binding protein, Eisenberg and colleagues (22) observed that residues 1 to 13 and 20 to 34 form helices in the absence of any lipids or other structure-promoting factors, in agreement with our localization of the first helical region. Overall, the different methods (chemical shift analysis, sequence-based prediction, and sequential NOEs) provide a reasonably consistent picture of the oligomer in solution: that the monomer unit of the αSyn oligomer consists of two regions that fractionally occupy helical structures (α1–α2) spanning the first 103 residues followed by a disordered C-terminal region. We note that the micelle-associated αSyn hairpin structure described by Ulmer et al. (15) contains similar helical regions (Val-3-Val-37 and Lys-45-Thr-92).

To determine the relative arrangement of monomers within the oligomer, we introduced the spin label 1-oxyl-2,2,5,5-tetramethylpyrroline-3-methyl-methanethiosulfonate (MTSL) at residue 9

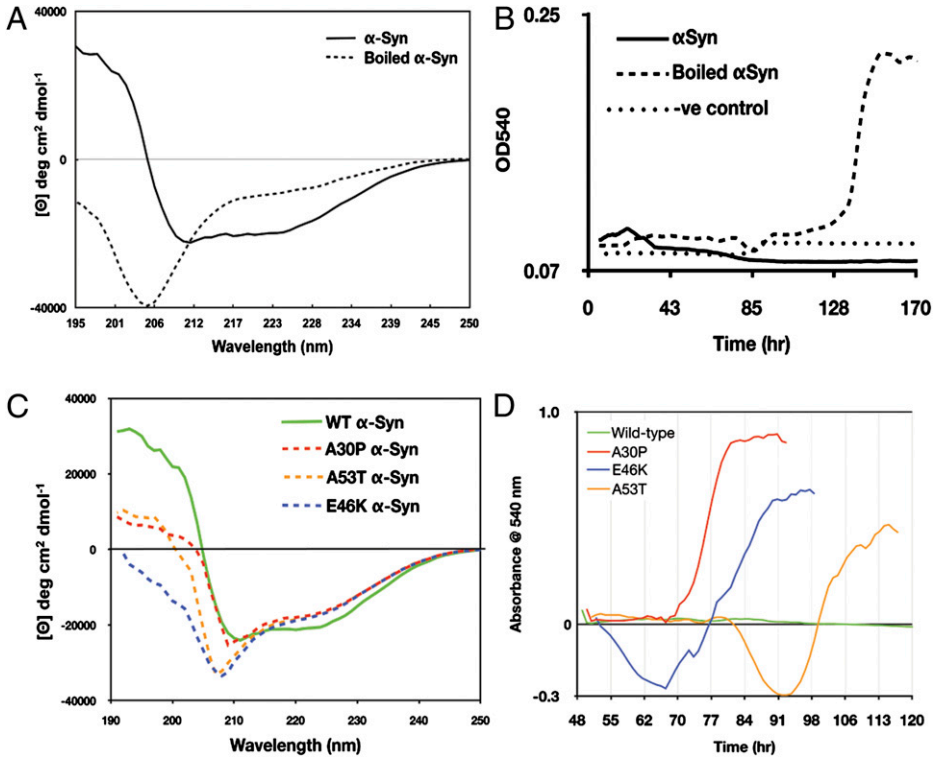

Fig. 3. Secondary structure and aggregation of αSyn. (*A*) Circular dichroism (CD) spectrum of αSyn before (solid line) and after boiling (dotted line). (*B*) Congo red aggregation assay of αSyn (solid line), boiled αSyn (dashed line), and buffer control with no protein (dotted line). (*C*) CD spectrum of αSyn wild-type (solid green), mutants A30P (red dashed line), A53T (orange dash), and E46K (blue dash). (*D*) Congo red aggregation assay of wild-type αSyn (green), A30P (red), E46K (blue), and A53T (orange).

after mutating it from serine to cysteine. Mixing of spin-labeled natural abundance S9C αSyn with ^{15}N-labeled wild-type αSyn in ratios of 1:3, 1:2, 1:1, 2:1, and 3:1 resulted in increased paramagnetic relaxation effects (PRE) for multiple backbone ^{15}N-^{1}H correlations assigned to residues in the α1, α2, and interhelical regions, with little or no effects on the C-terminal region. These intermolecular PREs (*SI Appendix*, Fig. S8) can be summarized as follows. Within the α1 and α2 regions, the largest effects are observed in α1 close to the N terminus, consistent with a parallel arrangement of monomers within a dynamic oligomer, and vary sequentially in a manner consistent with at least partial protection within helical secondary structure. Effects in the α2 region are smaller in magnitude than those in α1, with a broad effect between residues 70 and 107 with a maximum broadening (i.e., minimum signal) near Val-82; this is consistent with decreased solvent exposure for α2 relative to α1 as well as an antiparallel arrangement of the α1 and α2 regions within a monomer. ^{15}N-edited TOCSY spectra of the same samples showed extensive broadening of side chain ^{1}H resonances assigned to Asp2-Met5 and Gly7-Lys10, also consistent with a parallel arrangement of monomers. Significant broadening is observed for side chain resonances for Thr92 and the α-protons of Gly93. Considerable broadening effects of spin label at S9C are also observed for the backbone NH correlations of residues 37 to 42 at the end of the α1 region, as well as the side chain ^{1}H resonances of Val-48 and His-50 at the N terminus of the α2 region. These residues form part of a loop that has been found to interact with lipophilic compounds (7, 23), so it is possible that these effects are due to interoligomer interactions.

The NH correlations of a ^{15}N-labeled sample of αSyn cross-linked with glutaraldehyde showed significant changes in the HSQC (fingerprint) profile, mostly in the regions containing helical structure, with little or no change in the disordered C-terminal tail (residues 98–140) (*SI Appendix*, Fig. S9). A nonreducing SDS/PAGE of the cross-linked NMR sample exhibited four distinct bands, confirming that a tetrameric species was the highest-order oligomer present in significant concentration in the cross-linked sample.

Effects of Detergent, Concentration, and Heat Denaturation. To investigate whether oligomerization of αSyn is driven by the presence of BOG, we performed size-exclusion chromatography, cross-linking, and CD in buffer without BOG or glycerol and observed no difference compared with samples with BOG (*SI Appendix*, Figs. S10 and S11). ^{1}H,^{15}N HSQC spectra obtained without BOG also retained the same appearance as with the surfactant present. We also tested for the presence of bacterial lipids by analyzing the total phosphorus content in our αSyn samples and found no difference with negative controls.

Heat treatment of our αSyn preparation at 95 °C resulted in the formation of white precipitate after 10 min. The precipitate redissolves after mixing. However, boiled samples appear to be mostly disordered by CD (Fig. 3*A*), and the HSQC NMR spectrum of boiled αSyn is consistent with that of a disordered protein (*SI Appendix*, Fig. S12). NMR-based diffusion measurements performed on boiled and unboiled tetramer samples are consistent with decreased oligomerization and increased mobility of the boiled material. The diffusion coefficient was calculated to be $3.07 \pm 0.06 \times 10^{-5}$ cm^2/s for nonboiled and $3.38 \pm 0.05 \times 10^{-5}$ cm^2/s for boiled 0.1 mM αSyn, suggesting a statistically significant difference in mobility. The diffusion coefficients of buffer constituents did not change significantly for either sample ($1.60 \pm 0.01 \times 10^{-4}$ cm^2/s). We also found that the oligomeric state of αSyn is sensitive to protein concentration: CD spectra of recombinant αSyn at concentrations below 0.5 mg/mL appeared as mostly disordered protein. Similarly, the ^{1}H,^{15}N HSQC spectrum of a dilute (50 μM) sample of the αSyn construct yielded a spectrum similar in appearance to that of the boiled material, that is, broadening of resonances assigned to the first 100 residues, whereas the C-terminal residues are largely unperturbed (*SI Appendix*, Fig. S13). These data suggest that low levels of expression in recombinant experiments, or dilution of the sample on cell lysis, purification, and/or storage, could shift the equilibrium between monomer and oligomer in favor of the former.

Amyloidosis and Cytotoxicity. Though αSyn forms fibrils readily, αSyn as prepared herein is resistant to fibrillation. A Congo red assay showed that boiled αSyn samples began to aggregate on day 4 with maximum aggregation on day 5 (Fig. 3*B*). In contrast, unboiled samples did not form detectable aggregates, even after 2 wk at ambient temperature. Clearly, heat treatment of oligomeric αSyn makes it more aggregation prone. If this in vitro observation reflects the in vivo situation, then tetrameric αSyn in the cell must undergo a transformation during the course of amyloidosis similar to that induced by heating.

αSyn is also known to form pores in membranes, but tetrameric αSyn does not perforate membranes. Our αSyn preparation binds to liposomes, as reported in the literature for conventionally prepared αSyn (*SI Appendix*, Fig. S14). However, the liposome's permeability for potassium, sodium, and calcium ions does not change upon binding of the αSyn construct. Furthermore, we found no toxic effects upon addition of tetrameric αSyn to neuronal tissue culture, even at high concentrations (*SI Appendix*, Fig. S15), suggesting that this species does not disrupt organelle membranes and is not toxic to cells (8, 24).

Consequences of Disease-Associated Mutations. All three disease-associated mutants were purified and analyzed by CD. All three mutations rendered the protein more disordered under the same concentration and buffer conditions as wild-type protein (Fig. 3*C*). Structural perturbation was most pronounced in the A30P mutant where its CD spectrum was shifted toward extended structure. In contrast to WT, all three mutants aggregated readily based on a Thioflavin-T and Congo red aggregation assay (Fig. 3*D*), with A30P aggregating most rapidly. This finding is in contrast with reports in the literature where A30P, presumably in monomeric form, was shown to aggregate more slowly than wild-type protein (25).

Discussion

We have identified and characterized a soluble tetramer of αSyn that fractionally occupies a helical secondary structure as determined by CD and NMR. The formation of a secondary structure in the absence of lipids or micelles is likely in response to intersubunit hydrophobic interactions that drive oligomer formation, as has been observed for other intrinsically disordered proteins (26). Indeed, ^{1}H,^{15}N-HSQC spectra of dilute (50 μM) αSyn construct show clear correlations only for the C-terminal residues, suggesting an increase in dynamic broadening due to an equilibrium between more compact and extended forms of the protein at low concentrations. The pattern of intermonomer paramagnetic broadening effects observed in mixed samples prepared from monomer that is spin labeled at residue 9 with ^{15}N-labeled WT monomer indicates that a parallel orientation of monomers is preferred in the tetramer, with the N-terminal region forming the exterior of the oligomer. However, the extent of the broadening, along with the fact that monomer exchange takes place on the time scale of the NMR experiment, is further evidence that the tetramer is dynamic.

Though the αSyn construct we use differs from the native human αSyn in that it retains an extra 10 residues at the N terminus after removal of the GST tag used in purification, there is ample evidence that our observations and conclusions can reasonably be applied to wild-type αSyn as it occurs in vivo. For example, the similarity between the ^{1}H,^{15}N HSQC fingerprint of

our construct (*SI Appendix*, Figs. S2 and S3) with the in vivo NMR data from McNulty et al. (17) on WT αSyn argues that our construct provides a reasonable model for the behavior of WT αSyn. Further, WT αSyn isolated under nondenaturing conditions from neuronal and red blood cells behaves as a stable tetramer with properties, including helical content as estimated by CD, virtually identical to those of the recombinant protein reported here (9). Note that disease-related mutations (A30P, E46K, and A53T) markedly decrease the stability of the αSyn tetramer (Fig. 3).

The data presented here suggest that αSyn is like many other proteins whose structure depends on subunit concentration and environmental factors (26). In vitro, and probably in vivo, an equilibrium exists between unfolded monomer, compact oligomer, and (perhaps) amyloid-forming species. The unfolded form can be induced by heating, chemical treatment, or dilution, and our preliminary data also suggest that too high a concentration of αSyn appears to favor species with less helical content that, over time, aggregate into amyloid fibrils. Consistent with this picture, overexpression of αSyn in yeast leads to the formation of amyloid-like aggregates and cytotoxicity in a dose-dependent manner (27), and duplication and triplication of the WT *SNCA* locus in humans causes familial Parkinson disease with an age of onset that decreases with increasing number of copies of the gene (28).

Based on current evidence, we propose a simple model to fit the compact fourfold symmetrical structure observed in EM reconstructions (Fig. 4), with the caveat that the solution situation is clearly more complex and dynamic. Given that the α2 region would form an amphiphilic helix with the hydrophobic face consisting exclusively of valine residues, we expect that the α2 region forms the core of the complex. Antiparallel arrangement of α1 and α2 places the spin label in a position opposite from the portion of the α2 helix centered on Val-82 showing the largest PRE (*SI Appendix*, Fig. S8). We note that this antiparallel hairpin arrangement of α1 and α2 closely resembles the structure determined by Ulmer et al. (15) for micelle-associated αSyn determined using residual dipolar couplings. We are currently using residual dipolar couplings and heteronuclear relaxation measurements to better characterize the solution structure and dynamics of the αSyn tetramer.

To date, most αSyn research has focused on characterizing its aggregation properties and searching for the elusive toxic forms; less is known about its native structure and function. Here it is shown that αSyn can exist as a tetramer that is resistant to aggregation, and that perturbations caused by heating or disease-associated point mutations render it more aggregation prone. Taken together, these data suggest that structural perturbation, due to disease-associated point mutations or posttranslational modifications (aberrant proteolysis, oxidation, etc.), leading to destabilization of the tetramer and formation of a species that is more prone to aggregation, might constitute the mechanism of αSyn-associated disease pathogenesis. The ability to isolate αSyn as a stable oligomer that is not toxic to cells opens up the possibility that pharmacological stabilization of this structure may represent a unique approach to therapeutics for PD.

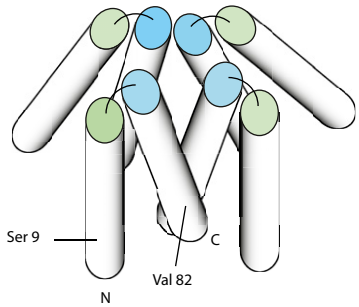

Fig. 4. Model for compact αSyn tetramer based on EM reconstruction and PRE. Helices are represented as cylinders. N indicates the N-terminal of the protein, with the first helix (α1, represented by green-ended cylinder) ending at ~residue 43. The second helix (α2, blue ended) starts ~residue 50 and ends at residue 103 (marked C). The remainder of the polypeptide, which is expected to be disordered, is not represented. The approximate position of Ser-9 (replaced by Cys for PRE experiments) and Val-82 (maximum PRE on α2) is shown.

Materials and Methods

Protein Expression and Purification. Construction of the expression vector used in this work is described in *SI Appendix*. The N-terminally fused GST-tagged protein was expressed in *E. coli* Rosetta2 strain (Novagen) during overnight induction (1 mM isopropyl β-D-thiogalactoside) at 20 °C. The Rosetta2 *E. coli* strain (Novagen) was selected as the expression host to facilitate expression, and induction was carried out at 20 °C to slow protein production and prevent inclusion body formation. The cells were ruptured mechanically with an emulsifier (Avestin), and the fusion protein purified by GST affinity chromatography on a glutathione-Sepharose column (Pharmacia). The N-terminal GST tag was removed by overnight digestion with Prescission protease (GE Biosciences) at 4 °C. Cleavage with Precission protease left 10 residues (GPLGSPEFPG) of the protease recognition site on the N-terminal of αSyn. αSyn was separated from the GST tag and uncleaved fusion on a glutathione-Sepharose column. The target protein was further purified by size-exclusion chromatography on a Sephacryl 200 HR column (GE Biosciences). The protein [100 mM Hepes (pH 7.4), 150 mM NaCl, 10% glycerol, 0.1% BOG] was concentrated to ~5 mg/mL (determined using absorbance at 280 nm and extinction coefficient of 5,960 $M^{-1}{\cdot}cm^{-1}$) and cleared through a 0.2-μm pore filter (Millipore). Protein yield was ~1 mg/L of LB culture. Protein was either used immediately or flash-frozen in liquid nitrogen and stored at −80 °C.

Size-Exclusion Chromatography. A set of low–molecular-weight protein standards (GE Biosciences) were run on a Superdex-75 column (GE Biosciences) under the same conditions used for purifying αSyn on an AKTA FPLC system (GE Biosciences). The molecular weight of αSyn was estimated using a linear regression analysis of K_{av}[(Ve − Vo)/(Vc − Vo)] vs. ln molecular weight. Ve is the elution volume of each standard, Vo is the void volume, and Vc is the column volume. For heat-denatured samples, 200 μL of 1 mg/mL of αSyn was heated at 95 °C for 10 min and cooled to room temperature before injection. For chemically denatured αSyn, 200 μL of 1 mg/mL αSyn was exchanged into 10 mM Tris·HCl and then lyophilized. The lyophilized αSyn was resuspended in 8 M urea and incubated at room temperature with agitation for 30 min before loading onto the column.

Chemical Cross-Linking. Cross-linking of purified αSyn and BE(12)M17 cell lysates were carried out with glutaraldehyde (Electron Microscopy Sciences). A total of 10 μL of cross-linker at various concentrations were added directly to 90 μL of protein solution at ~1 mg/mL containing 100 mM Hepes (pH 7.4), 150 mM NaCl, 10% glycerol, and 0.1% BOG, and agitated at 150 rpm (Eppendorf MixMate) and 37 °C for 30 min. The reaction was quenched with 10 μL 1 M Tris·HCl (pH 8). The apparent molecular weight of purified cross-linked αSyn on 12% SDS/PAGE (Fisher) and 4% to 16% gradient Blue Native PAGE (Invitrogen) was estimated using a linear regression analysis of protein standard retentions (Pierce).

Circular Dichroism. The protein solution was exchanged with 10 mM Tris·HCl (pH 7.4), 150 mM NaCl, and 10% glycerol, with and without 0.1% BOG, to a protein concentration ranging from 0.5 to 3 mg/mL as determined by absorbance at 280 nm. Control samples contained the same buffer without glycerol or BOG. CD spectra were collected on a Biologic Science Instruments MOS450 AF/CD spectrometer or a Jasco 810 spectrometer at 25 °C, path length 0.2 mm or 0.5 mm (depending on protein concentration), slit width 1.0 mm, and acquisition of 2.0 s. Secondary structure content was analyzed with the online DichroWeb server. The data used for graphical presentation and analyses were each an average of five different scans.

MALDI-TOF Mass Spectrometry. A total of 1 μL of sample was spotted on a MALDI target containing 1 μL of 20 mg/mL sinipic acid, and analyzed on a Bruker Daltonics UltrafleXtreme TOF/TOF. The MALDI was calibrated each time using a high–molecular-weight protein calibration standard, Protein Calibration Standard 1 (Bruker Daltonics), using gas phase dimers of standard proteins to extend the mass range of calibration. The MALDI-TOF was

operated in linear mode using a laser power of 72% to 90%, using the manufacturer provided LPHighMass program, with detector gain adjusted 70% above manufacturer's presets. MALDI-TOF spectra of cross-linked and non–cross-linked samples were analyzed using FlexAnalysis software (Bruker Daltonics).

Aggregation Assays. For Congo red assays, 1 mg of αSyn was added to 200 μL of 100 mM Hepes (pH 7.4), 150 mM NaCl, 10% glycerol, 0.1% BOG, and 1.5 μM Congo red and incubated at 37 °C with constant agitation. Absorbance at 540 nm was measured every 15 min for 7 d. For thioflavin T (ThT) assays, 0.6 mg of αSyn was added to 200 μL of 100 mM Hepes (pH 7.4), 150 mM NaCl, 10% glycerol, 0.1% BOG, and 5 μM ThT and incubated at 37 °C with frequent agitation. The fluorescence of ThT was measured with a FlexStation (Molecular Devices) at an excitation wavelength of 440 nm, an emission wavelength of 490 nm, and a cutoff wavelength of 475 nm.

Electron Microscopy and Image Analysis. EM specimens were prepared on carbon-coated 400-mesh copper-rhodium EM grids (Ted Pella) rendered hydrophilic by glow discharge in the presence of amylamine. Aliquots of αSyn (3 μL at ~35 ηg/μL) were adsorbed onto the grid during a 1-min incubation. The grids were then washed with water 3× and stained with 1% wt/vol uranyl acetate for 2 min. Imaging was performed on a Tecnai F-20 microscope at an acceleration of 120 kV, 80,000× magnification, and ~800-nm underfocus. Images were recorded on a 4,096 × 4,096 pixel CCD camera (TVPIS GmbH) with twofold pixel binning. Individual CCD frames were normalized and Weiner filtered with the Appion processing package (29), and 18,761 individual particle images were automatically selected (30). Individual particle images were analyzed using the SPIDER and SPARX EM image processing packages (31, 32).

NMR Experiments. Samples of ^{15}N- and ^{13}C-labeled αSyn for NMR spectroscopy were prepared as described above except that the bacteria were cultured using uniformly ^{13}C- and ^{15}N-labeled media (Spectra 9; Cambridge Isotope Laboratories). NMR samples were typically prepared to a final concentration of ~0.5 mM in 100 mM Tris·HCl (pH 7.4), 100 mM NaCl, 0.1% β-octyl-glucoside, 10% glycerol, and 10% D_2O. All NMR spectroscopy was performed on a Bruker Avance 800 NMR spectrometer operating at 800.13 MHz (^{1}H), 81.08 MHz (^{15}N), and 201.19 MHz (^{13}C) and equipped with a TXI cryoprobe and pulsed-field gradients. Experiments used for sequential resonance assignments include 3D experiments HNCA, HNCACB, ^{15}N-HSQC TOCSY, and ^{15}N-HSQC NOESY. Quadrature detection was obtained in the ^{15}N dimension of 3D experiments using sensitivity-enhanced gradient coherence selection (33), and in the ^{13}C dimension using States-TPPI, with coherence selection obtained by phase cycling. In all cases, spectral widths of 8,802.82 Hz (^{1}H) and 2,920.56 Hz (^{15}N) were used. For ^{13}C, spectral widths of 6,451.61 Hz (HNCA) and 15,105.74 Hz (HNCACB) were used. All experiments were performed at 298 K unless otherwise noted. NMR data were processed using TOPSPIN (Bruker Biospin Inc.), and data analyzed using either TOPSPIN or SPARKY (34). Random coil chemical shift predictions were made using CamCoil (http://www-vendruscolo.ch.cam.ac.uk/camcoil.php) (19). Fractional helix occupancies were calculated by the method of Yao et al. (21).

Experimental conditions for pulsed field gradient diffusion measurement, spin-labeling experiments, liposome assays, and cytotoxicity assays can be found in *SI Appendix*.

ACKNOWLEDGMENTS. We thank S. Lindquist for yeast expression vectors of αSyn; S. Subramanian for help collecting preliminary NMR data; S. Pochapsky for help with NMR experiments and processing data; C. Miller for assistance with liposome assays; M. Georgiadis for providing 1-ethyl-3-(3-dimethylaminopropyl)carbodiimide cross-linker; K. Dunker for access to CD; Clark Wells for the plate reader; N. Agar for use of her MALDI-TOF mass spectrometer; A. Hudmon for spectrofluorimeter access; and J. Sussman for helpful discussions. We also acknowledge the National Resource for Automated Molecular Microscopy. Support for this work was provided by the Michael J. Fox Foundation (Q.Q.H., D.R., and G.A.P.); an Indiana University School of Medicine Biomedical Research grant (to Q.Q.H.); a Fidelity Biosciences Research Initiative (with much useful discussion from Dr. S. Weninger) (to G.A.P. and D.R.); The Ellison Medical Foundation and The McKnight Endowment for Neuroscience; and a Rapid Response grant from the Michael J. Fox Foundation (to T.C.P. and I.P.). This research was supported in part by the Intramural Research Program of the National Institutes of Health, National Institute on Aging.

1. Goedert M (2001) Alpha-synuclein and neurodegenerative diseases. *Nat Rev Neurosci* 2:492–501.
2. Jellinger KA (2003) Neuropathological spectrum of synucleinopathies. *Mov Disord* 18 (Suppl 6):S2–S12.
3. Karpinar DP, et al. (2009) Pre-fibrillar alpha-synuclein variants with impaired beta-structure increase neurotoxicity in Parkinson's disease models. *EMBO J* 28:3256–3268.
4. Klockgether T (2004) Parkinson's disease: Clinical aspects. *Cell Tissue Res* 318(1): 115–120.
5. George JM, Jin H, Woods WS, Clayton DF (1995) Characterization of a novel protein regulated during the critical period for song learning in the zebra finch. *Neuron* 15:361–372.
6. Cooper AA, et al. (2006) Alpha-synuclein blocks ER-Golgi traffic and Rab1 rescues neuron loss in Parkinson's models. *Science* 313:324–328.
7. Volles MJ, Lansbury PT, Jr. (2002) Vesicle permeabilization by protofibrillar alpha-synuclein is sensitive to Parkinson's disease-linked mutations and occurs by a pore-like mechanism. *Biochemistry* 41:4595–4602.
8. Kim HY, et al. (2009) Structural properties of pore-forming oligomers of alpha-synuclein. *J Am Chem Soc* 131:17482–17489.
9. Bartels T, Choi JG, Selkoe DJ (2011) α-Synuclein occurs physiologically as a helically folded tetramer that resists aggregation. *Nature* 477(7362):107–110.
10. Wittig I, Beckhaus T, Wumaier Z, Karas M, Schägger H (2010) Mass estimation of native proteins by blue native electrophoresis: Principles and practical hints. *Mol Cell Proteomics* 9:2149–2161.
11. Conway KA, Harper JD, Lansbury PT, Jr. (2000) Fibrils formed in vitro from alpha-synuclein and two mutant forms linked to Parkinson's disease are typical amyloid. *Biochemistry* 39:2552–2563.
12. Sreerama N, Woody RW A self-consistent method for the analysis of protein secondary structure from circular dichroism. *Anal Biochem* 209(1):32–44.
13. Provencher SW, Glöckner J (1981) Estimation of globular protein secondary structure from circular dichroism. *Biochemistry* 20(1):33–37.
14. Nettleship JE, Brown J, Groves MR, Geerlof A (2008) Methods for protein characterization by mass spectrometry, thermal shift (ThermoFluor) assay, and multiangle or static light scattering. *Methods Mol Biol* 426:299–318.
15. Ulmer TS, Bax A, Cole NB, Nussbaum RL (2005) Structure and dynamics of micelle-bound human alpha-synuclein. *J Biol Chem* 280:9595–9603.
16. Chandra S, Chen XC, Rizo J, Jahn R, Südhof TC (2003) A broken alpha -helix in folded alpha-Synuclein. *J Biol Chem* 278:15313–15318.
17. McNulty BC, Young GB, Pielak GJ (2006) Macromolecular crowding in the *Escherichia coli* periplasm maintains alpha-synuclein disorder. *J Mol Biol* 355:893–897.
18. Shen Y, Delaglio F, Cornilescu G, Bax A (2009) TALOS+: A hybrid method for predicting protein backbone torsion angles from NMR chemical shifts. *J Biomol NMR* 44:213–223.
19. De Simone A, Cavalli A, Hsu STD, Vranken W, Vendruscolo M (2009) Accurate random coil chemical shifts from an analysis of loop regions in native states of proteins. *J Am Chem Soc* 131:16332–16333.
20. Schwarzinger S, Mohana-Borges R, Kroon GJA, Dyson HJ, Wright PE (2008) Structural characterization of partially folded intermediates of apomyoglobin H64F. *Protein Sci* 17:313–321.
21. Yao J, Chung J, Eliezer D, Wright PE, Dyson HJ (2001) NMR structural and dynamic characterization of the acid-unfolded state of apomyoglobin provides insights into the early events in protein folding. *Biochemistry* 40:3561–3571.
22. Zhao ML, Cascio D, Sawaya MR, Eisenberg D (2011) Structures of segments of α-synuclein fused to maltose-binding protein suggest intermediate states during amyloid formation. *Protein Sci* 20:996–1004.
23. Liu ZH, et al. (2009) Membrane-associated farnesylated UCH-L1 promotes alpha-synuclein neurotoxicity and is a therapeutic target for Parkinson's disease. *Proc Natl Acad Sci USA* 106:4635–4640.
24. Danzer KM, et al. (2007) Different species of alpha-synuclein oligomers induce calcium influx and seeding. *J Neurosci* 27:9220–9232.
25. Li J, Uversky VN, Fink AL (2001) Effect of familial Parkinson's disease point mutations A30P and A53T on the structural properties, aggregation, and fibrillation of human alpha-synuclein. *Biochemistry* 40:11604–11613.
26. Danielsson J, et al. (2008) The intrinsically disordered RNR inhibitor Sml1 is a dynamic dimer. *Biochemistry* 47:13428–13437.
27. Outeiro TF, Lindquist S (2003) Yeast cells provide insight into alpha-synuclein biology and pathobiology. *Science* 302:1772–1775.
28. Fuchs J, et al. (2007) Phenotypic variation in a large Swedish pedigree due to SNCA duplication and triplication. *Neurology* 68:916–922.
29. Lander GC, et al. (2009) Appion: An integrated, database-driven pipeline to facilitate EM image processing. *J Struct Biol* 166(1):95–102.
30. Voss NR, Yoshioka CK, Radermacher M, Potter CS, Carragher B (2009) DoG Picker and TiltPicker: Software tools to facilitate particle selection in single particle electron microscopy. *J Struct Biol* 166:205–213.
31. Hohn M, et al. (2007) SPARX, a new environment for Cryo-EM image processing. *J Struct Biol* 157(1):47–55.
32. Frank J, et al. (1996) SPIDER and WEB: Processing and visualization of images in 3D electron microscopy and related fields. *J Struct Biol* 116:190–199.
33. Kay LE, Keifer P, Saarinen T (1992) Pure absorption gradient enhanced heteronuclear single quantum correlation spectroscopy with improved sensitivity. *J Am Chem Soc* 114:10663–10665.
34. Goddard TD, Kneller DG (2008) SPARKY 3 (University of California, San Francisco).